



pubs.acs.org/acsaom Article

# Anisotropic Two-Photon Excited Photoluminescence and Optical Constants of InGaN Nanowires

Emma M. Sundin, <sup>¶</sup> Debabrata Das,\*, <sup>¶</sup> Kausik Kolluri, Pallab Bhattacharya, Chintalapalle V. Ramana, and Chunqiang Li\*



Cite This: ACS Appl. Opt. Mater. 2023, 1, 973-981

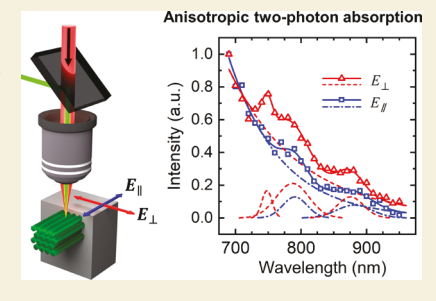


ACCESS

III Metrics & More

Article Recommendations

ABSTRACT: Gallium nitride (GaN) and its derivatives are important materials for optoelectronic and electronic applications, such as light-emitting diodes, solid-state lasers, optical modulators, artificial photosynthesis, etc. Controlled growth and manipulation of these materials at nanoscale dimensions and understanding their linear and nonlinear optical properties lay the foundation for developing next-generation optoelectronic and electronic devices. In this context, herein, we report on the two-photon absorption and anisotropic two-photon excited photoluminescence of InGaN (IGN) nanowires grown by molecular beam epitaxy. The IGN nanowires were imaged using a home-built two-photon photoluminescence microscope with a tunable femtosecond laser to excite over the near-IR range (690–950 nm). In addition, the polarization angle of the excitation electric field



was also rotated, and the emitted photoluminescence was analyzed with a polarizer. Results showed polarized photoluminescence with a stronger signal in the direction perpendicular to the IGN nanowires' axis. Also, we observed strong two-photon absorption above the bandgap, with several excitation spectrum peaks near 740, 790, and 870 nm. These peaks showed anisotropic response to the excitation polarization angle, which may be due to the anisotropy of the IGN nanowires' wurtzite phase. The polarized light absorption and emission nature of IGN nanowires, as revealed in this work, may be useful for optimizing materials for future optoelectronic device applications.

KEYWORDS: InGaN nanowires, two-photon absorption, anisotropy, optical constants, spectroscopic ellipsometry

## 1. INTRODUCTION

Gallium nitride (GaN) has been widely used as the semiconductor platform for electronic and optoelectronic applications.  $^{1-3}$  Adding indium (In) to GaN to form ternary InGaN (IGN) can systematically tune the semiconductor bandgap, thus leading to broad applications.  $^{4,5}$  One challenge is the large lattice mismatch between GaN and InN ( $\sim$ 10%), which makes it difficult to grow high-quality InGaN crystals. One approach to relax this mechanical strain is to utilize the nanowire structure, which has demonstrated high quantum efficiency for optoelectronic device applications.  $^{6-9}$  Overall, these group-III-nitride nanowires, particularly IGN nanowires, are promising candidates for optoelectronic and light energy harvesting applications.  $^{10,11}$ 

In nanowires' photonic applications, one important aspect is the presence of polarization-related optical phenomena, i.e., the light emitted or absorbed by nanowires depends on the orientation of the nanowires. Such polarization-sensitive phenomena originate from both atomic and macroscale anisotropy. The IGN nanowires are typically grown in the hexagonal wurtzite (WZ) structure, where the *c*-axis is along the nanowire axis. This WZ structure is thermodynamically stable and has uniaxial symmetry. Thus, the electronic band structure of WZ semiconductors is inherently anisotropic,

which results in anisotropic electric dipole transitions along and normal to the hexagonal axis. Nanowires with diameters on the order of several nanometers will show a quantum confinement effect on the electron energy levels in the normal direction of nanowires. When nanowires' diameters are on the order of tens of nanometers, such a quantum effect is minimal. Instead, the dielectric constant mismatch between the nanowires and their environment is anisotropic. 17,18

Nonlinear optical phenomena have a broad range of applications in modern technologies, such as optical communication and quantum information. <sup>19</sup> Nanostructures have great advantages over bulk or thin-film materials due to their small scale and flexibility to be fabricated by design, e.g., metamaterials. Optical absorption and photoluminescence (PL) spectroscopic studies of nanowires have revealed energy levels, quantum transitions, and the influence of size. <sup>20–22</sup> The IGN nanowires and quantum dots are potential candidates for

Received: January 27, 2023 Accepted: April 20, 2023 Published: May 2, 2023





integrated nonlinear optical devices directly grown on silicon.  $^{6-8,23}$  Preliminary studies on second harmonic generation and two-photon excitation in InGaN/GaN materials have revealed the absorption bands and crystallographic orientation.  $^{24-26}$  In this work, we examined the two-photon PL excitation (PLE) spectra of IGN nanowires under different excitation light polarizations and also studied the polarization of the emitted light (Figure 1). Our results revealed the

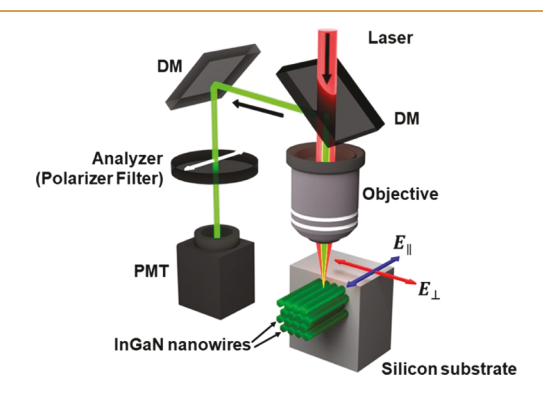


**Figure 1.** Two-photon PL microscopy setup. DM: dichroic mirror, PMT: photomultiplier tube.

anisotropic resonant excitation of nanowires under normal and parallel directions to nanowires. The polarized light absorption and emission nature of IGN nanowires, as presented and discussed in this paper, may be useful for optimizing materials for future optoelectronic device applications. Furthermore, because efforts on using ellipsometry studies or establishing optical constants of IGN nanowires are scanty in the literature, we performed comprehensive spectroscopic ellipsometry (SE) studies. The primary advantage of SE is its ability to determine the material's complex dielectric function, which provides crucial information about the material's optical properties. Therefore, we believe that the dispersion behavior of optical constants and dielectric function, along with the two-photon absorption measurements, make the study complete and useful for considering these IGN nanowires for optical and optoelectronic device applications.

# 2. MATERIALS AND METHODS

#### 2.1. IGN Nanowire Growth

The IGN nanowires with an areal density of  $10^{10}$  to  $10^{11}$  cm<sup>-2</sup> were grown on an n<sup>+</sup> Si(111) substrate in a plasma-assisted molecular beam epitaxy system. <sup>6,8,9,23,27</sup> The Si substrate was thoroughly cleaned with acetone, isopropanol, and DI water for 10 min each. Then the substrate was dipped into a buffered HF solution for oxide removal. Inside the lode-lock and buffer chambers, the substrate was heated at 200 and 500 °C to remove water vapor and organic contaminants, respectively. In the growth chamber, the substrate was first heated up to 900 °C for oxide desorption and then cooled down to 800 °C. At this temperature, the growth was initiated with Ga droplets, followed by ~5–10 nm GaN nanowire nucleation layer. After that, the substrate temperature was lowered to 600 °C to grow IGN nanowires. Throughout the growth process, a constant N<sub>2</sub> flux of 1 sccm was maintained for the N<sub>2</sub> rich growth regime. Ga and In fluxes were kept at  $1.18 \times 10^{-7}$  and  $6.5 \times 10^{-8}$  Torr to get the desired green emission. The chamber pressure was  $8 \times 10^{-6}$  Torr during the growth process.

## 2.2. Characterization

**2.2.1. Scanning Electron Microscopy.** A Hitachi SU8000 cold field emission scanning electron microscope was employed to image the surface morphology of as-grown IGN nanowires. The sample was

fixed on a 45° slant sample holder to get a bird's-eye view of the IGN nanowires.

- **2.2.2.** X-ray Diffraction. The IGN nanowires were analyzed using X-ray diffraction (XRD) with a Malvern Panalytical Empyrean Nano edition multipurpose X-ray diffractometer in Bragg–Brentano reflection geometry. The  $\theta/2\theta$  scan was performed using a Cu K $\alpha$  X-ray source (0.154 nm) with a step size of 0.01° and an integration time of 0.6 s/step.
- **2.2.3. Absorbance/Reflectance.** Reflectance measurements were made using a V-770 UV—visible/NIR spectrophotometer (Jasco Inc.) in integrating sphere mode for thin films. The Kubelka—Munk (KM) model was then used to calculate an approximate absorbance spectrum of the IGN material. The KM formalism, <sup>28</sup> which proved to be quite useful to study the optical and optoelectronic materials, <sup>29</sup> was applied to calculate the absorption data of IGN nanowires from its diffused reflectance spectrum. The KM function is defined as <sup>28</sup>

$$F(R) = \frac{K}{S} = \frac{(1 - R)^2}{2R} \tag{1}$$

Here, F(R), K, S, and R represent the KM function, absorption coefficient, scattering coefficient, and reflectance, respectively.

- **2.2.4. Spectroscopic Ellipsometry.** The SE measurements were done using a Semilab SE-2000 at a 70° incident photon angle under atmospheric conditions. The experimental parameters, namely the angles  $\Psi$  (azimuth) and  $\Delta$  (phase change), were measured. By measuring these relative changes in the amplitude and phase of the linearly polarized monochromatic incident light upon oblique reflection from the IGN sample surface, appropriate models were used to investigate the optical constants of the IGN nanowires. The spectroscopic data were analyzed and modeled in Analyzer v1.6.6.2.
- **2.2.5. One-Photon PL.** For one-photon PL measurements, the sample was excited at room temperature using 325 nm photons from a He–Cd laser. The emitted signal was passed through a monochromator with 0.03 nm resolution and detected by a photomultiplier tube (PMT) detector.
- 2.2.6. Two-Photon PL. The nonlinear optical properties of the samples were investigated at room temperature using a two-photon PL microscope developed and built in-house by the UTEP Photonics Laboratory. A tunable IR laser source (Mai Tai HP, Spectra-Physics) was used to excite the nanowires; the emitted light was collected by a 60×/1.20 NA water-immersion objective (Olympus). Image resolution of the above setup was 0.67  $\mu m/pixel$ . The instrument's green channel (542/27 nm bandpass, Semrock) was used for two-photon PL analyses. To image the nanowires from the side, the substrate was mounted vertically on a metal block, and a glass coverslip was secured over the block and substrate edges. To investigate polarization excitation anisotropies, a multi-mirror setup was built to control the angle of polarized light entering the microscope and orient the excitation E-field parallel or perpendicular to the nanowire growthdirection axis (see red and blue arrows in Figure 1). Two-photon excitation spectroscopy was performed across 690-950 nm at 10 nm intervals using approximately 4 mW of excitation power at the sample. For each scan, two spectra were captured using excitation polarization perpendicular  $(E_{\perp})$  and parallel  $(E_{\parallel})$  to the nanowire, as described above. Data analysis was performed using ImageJ, MATLAB, and custom Python scripts. Raw micrographs were backgroundsubtracted, sectioned into regions, and the mean intensity value extracted for each wavelength and polarization state. Mid-sized (10 pixels wide regions, ~200 nanowires) and small (1 pixel wide regions, ~20 nanowires) ensembles were analyzed. To compensate for small amounts (<1  $\mu$ m) of sample movement in the normal direction of the substrate that occurred during scanning, regions were averaged over  $\sim$ 3 pixels in this dimension.

#### 3. RESULTS AND DISCUSSION

Scanning electron microscopy (SEM) images revealed the hexagonal cross-section of these IGN nanowires with a diameter of about 30-50 nm, height of about 300 nm, and density of about  $300/\mu m^2$  (Figure 2a). This hexagonal cross-

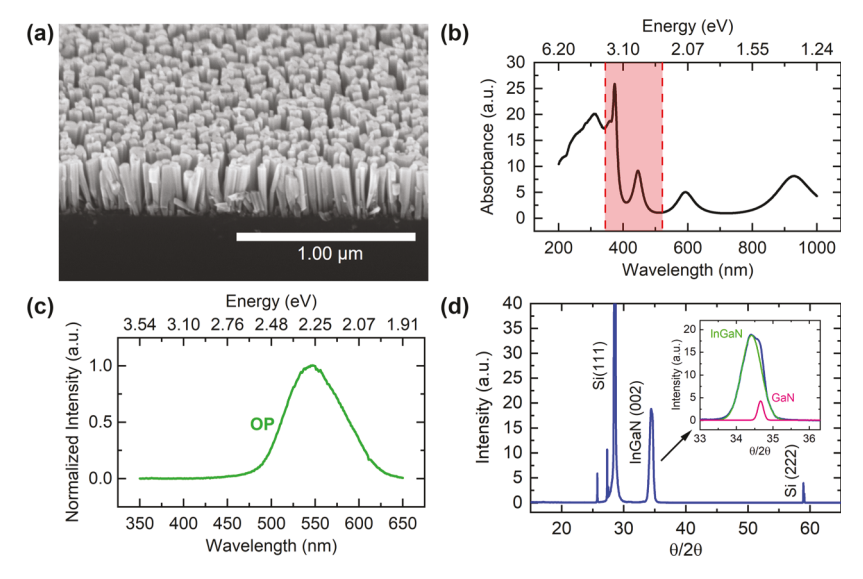


Figure 2. IGN nanowire characterization. (a) SEM image. (b) Absorption spectrum determined from reflectance measurements using the KM model, with corresponding range of the two-photon excitation spectrum marked in red shade (details in Figure 5). (c) One-photon PL emission spectrum. (d) XRD pattern.

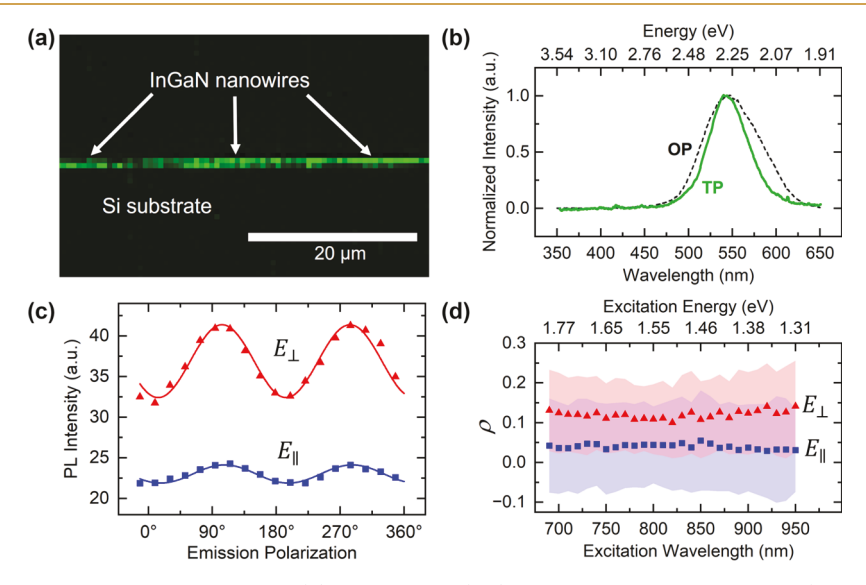


Figure 3. (a) Two-photon PL image of IGN nanowires. (b) Two-photon (TP) excited PL emission spectrum (solid line) vs one-photon (OP) excited PL spectrum (dash line) of the nanowires. (c) Polarized PL intensity under parallel (blue squares) and perpendicular (red triangles) excitation with a rotating polarizing analyzer. Zero degree is the direction parallel to the nanowires' axis. The two lines are fitting curves using a sine function. (d) Polarized anisotropic PL intensity ( $\rho$ ) from 690 to 950 nm. The red triangles and blue squares are averaged values of raw data points for perpendicular and parallel excitation, respectively, and the shaded regions indicate error bars ( $\pm \sigma$ , standard deviation).

section indicates these nanowires grow along the *c*-axis, which is perpendicular to the surface of the Si substrate, with a maximum deviation angle from the normal direction of less than 20°. The XRD pattern, shown in Figure 2d, indicates the monocrystalline nature of as-grown IGN nanowires. The dominant peak corresponding to (002) orientation is due to the growth along the *c*-axis. A high-resolution scan around the primary (002) peak (shown in the inset) identified the peaks corresponding to the seed GaN layer and the IGN nanowires. The reflectance absorption spectrum showed several distinct absorption peaks appearing at 311 nm (3.99 eV), 360 nm (3.44 eV), 373 nm (3.32 eV), 446 nm (2.78 eV), 592 nm (2.09 eV), and 929 nm (1.33 eV) (Figure 2b). The peak at 360 nm corresponds to the band gap of GaN, which is the buffer layer (~5–10 nm thickness) for growing IGN nanowires on Si

substrates. Absorption peaks at longer wavelengths are most likely due to nanowire absorption. Of particular interest are the two peaks at 373 and 446 nm, as these energy levels fall in the two-photon excitation wavelength range in this work (red shade). One-photon PL spectrum showed a peak at 547 nm (2.27 eV), with full width at half-maximum (FWHM) of 76 nm (Figure 2c). Compared with literature values, this emission peak wavelength suggests an In concentration of approximately x = 0.3 for  $\text{In}_x\text{Ga}_{1-x}\text{N}$  system (x = 0.28-0.43 based on Hahn et al.<sup>30</sup> and x = 0.25-0.3 based on Kuykendall et al.<sup>31</sup>).

Under two-photon excitation at a wavelength of 730 nm, these nanowires also showed strong PL signals (Figure 3a). This is a side view of nanowires with a Si substrate in the bottom half. The pixel size in this image is about 600 nm, thus each pixel contains about 20 nanowires. This resolution is

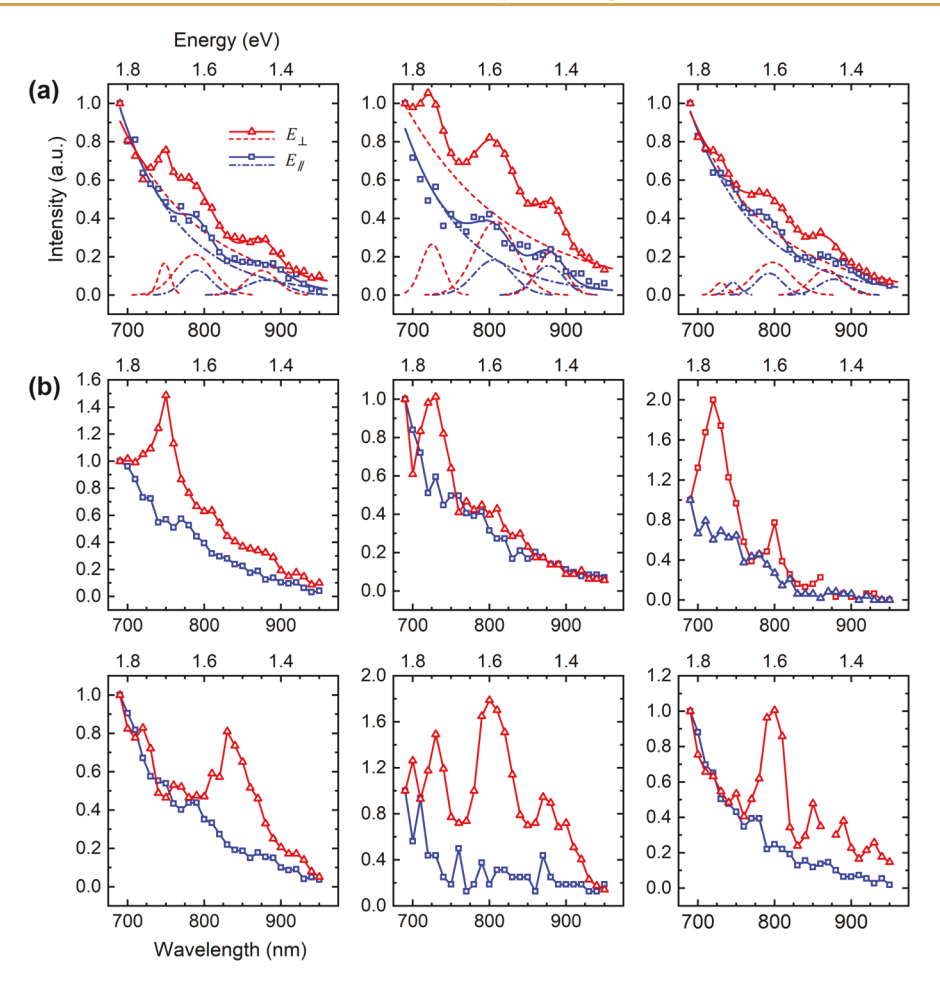


Figure 4. Two-photon PL excitation spectra from 690 to 950 nm with different polarizations  $E_{\perp}$  (red) and  $E_{\parallel}$  (blue). (a) PLE spectra of ~200 nanowires. Raw data (open triangles and squares), fitting sum result (solid lines), and background and peak components (dashed lines). (b) PLE spectra of one single-pixel wide regions from the raw images (~20 nanowires).

determined by the sampling rate of the electronics while the laser beam is scanning across the sample. The actual optical resolution is determined by the Abbe diffraction limit  $\sim$ 0.6  $\lambda$ / NA, which is about 200-300 nm. The two-photon excited PL spectrum was measured with a spectrometer (Ocean Optics, FLAME), as shown in Figure 3b. Basically, this spectrum is very similar to the one-photon PL spectrum (Figure 2c), with a peak at about 540 nm. Clearly, there are differences between the one-photon and two-photon excited PL spectra. The most noticeable one is that the FWHM of the two-photon PL spectrum (solid line) is only about 55 nm, while the FWHM of the one-photon spectrum (dash line) is about 76 nm. Also, there are different small peaks in both spectra. Such differences have been observed in other nanomaterials.<sup>32</sup> The origin of these differences is most likely due to different quantum pathways. First, electrons will be excited from the valence band into the conduction band. In the one-photon experiment, the excitation laser has a wavelength of 325 nm, while the twophoton excitation laser wavelength is at 710 nm. Also, the quantum selection rules are different for one-photon and twophoton absorptions. In two-photon absorption, the extra photon carries extra angular momentum, thus electrons will be excited into different energy levels from one-photon absorption. Further relaxation and radiative recombination processes could also be different between one-photon and two-

photon excited electrons and holes. Detailed investigation on this topic is beyond the scope of this work.

Analyzing the PL polarization with a polarizer in front of the PMT showed that the emitted light intensity was higher when the emitted light was perpendicular to the nanowire c-axis under both parallel  $(E_{\parallel})$  and perpendicular  $(E_{\perp})$  excitation with the same laser power (Figure 3c). One thing to notice is that the emission intensity under parallel excitation was lower than that under perpendicular excitation. The degree of anisotropy on the emission polarization angle can be quantified using the equation

$$\rho = (I_{\perp} - I_{\parallel})/(I_{\perp} + I_{\parallel}) \tag{2}$$

where  $I_{\perp}$  and  $I_{\parallel}$  are emission intensities when emitted light is perpendicular or parallel to the nanowire axis, respectively. Under perpendicular excitation  $(E_{\perp})$ ,  $\rho$  is about 0.13 compared to about  $\rho=0.05$  under parallel excitation  $(E_{\parallel})$  at the 700 nm excitation wavelength. When the excitation wavelength was scanned from 690 to 950 nm, this anisotropic emission was found to be consistent throughout the range by analyzing hundreds of single-pixel values in the raw images (Figure 3d). Because these nanowires have large diameters (30–50 nm), it is expected that the quantum confinement effect is minimal and that the classical effect (dielectric constant mismatch) and crystal structure anisotropy would contribute to this polarization anisotropy. The dielectric constant mismatch will lead

Table 1. Summary of Fitted Parameters for Two-Photon Excitation Spectroscopy PL Intensity Data

Parameter		$\lambda_{excitation}  (nm)$	Energy (eV)	FWHM (nm)	Intensity (a.u.)	$\rho = \left(\frac{I_{\perp} - I_{\parallel}}{I_{\perp} + I_{\parallel}}\right)$	
Peak 1	$E_{\perp}$ $E_{\parallel}$		734 746	1.69 1.66	23.9 15.7	0.167 0.0222	0.765
Peak 2	E _ //		797 796	1.55 1.56	60.3 47.4	0.256 0.142	0.286
Peak 3	E		874 879	1.42 1.41	45.5 52.5	0.162 0.105	0.211

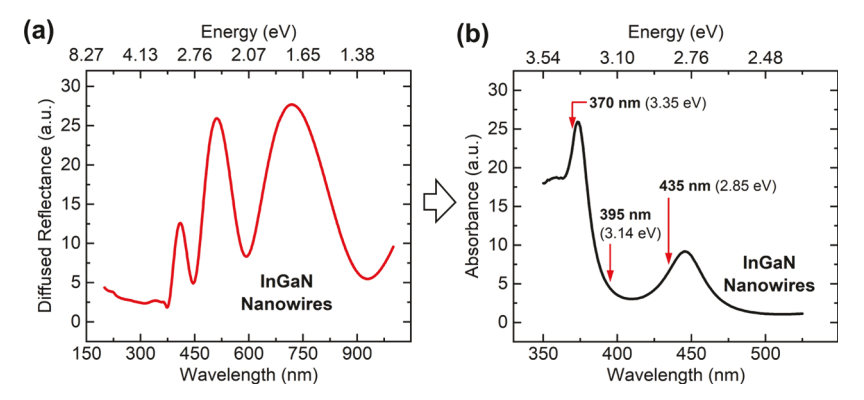


Figure 5. (a) Diffuse reflectance spectrum of IGN nanowires in the broad range of wavelengths. (b) One-photon absorption spectrum determined from reflectance measurements using the KM model, a subset of in the range of two-photon excitation PL spectra measured. Wavelengths are marked at the locations of peaks observed in two-photon excitation spectra.

to reduced emission intensity in the perpendicular direction,  $^{17,18}$  i.e.,  $I_{\perp} < I_{\parallel}$ , which is contrary to our observation here. Thus, this phenomenon of  $I_{\perp} > I_{\parallel}$  is most likely due to the energy splitting of ground states in wurtzite crystal. Also, donor- and acceptor-bound excitons can contribute to this polarization effect. More detailed studies are needed to examine the exact atomic-level origins of this anisotropy. In P nanowires with a diameter  $\sim 1~\mu \rm m$  in wurtzite phase also exhibit polarized emission perpendicular to the nanowire c-axis.  $^{34}$ 

We further scanned the two-photon excitation wavelength and polarization in the range of 690-950 nm to obtain the two-photon PLE spectra (Figure 4). Ensemble averaged spectra from different regions showed two-photon absorption above the IGN bandgap with three peaks near 740, 790, and 870 nm under both parallel and perpendicular polarizations  $(E_{\parallel} \text{ and } E_{\perp})$  (Figure 4a). Clearly, these PLE spectra are anisotropic among different polarizations. There were substantial sample variations among nanowires, which resulted in significant inhomogeneous broadening in spectral peaks. Therefore, the spectra from six distinct single-pixel signals in such images (~10 nanowires in linear dimension) are plotted in Figure 4b. The increased contrast and narrower peak widths are the expected result of reduced inhomogeneous broadening. Considerable variation in peak position (energy) and relative intensity was observed in this small-ensemble analysis, with some pixels clearly showing all three peaks and others only one or two strongly. The wider peaks seen in the larger ensembles (Figure 4a) are the result of averaging over the larger ~100nanowire regions. To quantify these spectra, we performed

Gaussian fitting with three peaks and a background exponential curve on both polarization data sets (Figure 4a). The fitted curves are plotted in Figure 4a, and quantitative results are listed in Table 1 with overall  $r^2 > 0.96$ . When the excitation electric field was perpendicular to the nanowire *c*-axis  $(E_{\perp})$ , all three peaks showed higher emission intensity than those when the excitation electric field was parallel to the nanowire c-axis  $(E_{\parallel})$ . Calculated  $\rho$  values for all three peaks are listed in Table 1, with  $\rho = 0.765$  for the peak near 740 nm,  $\rho = 0.286$  near 790 nm, and  $\rho = 0.211$  near 870 nm. The two peaks around 790 and 870 nm exhibited a similar level of anisotropy ( $\rho$ ) that was much lower than the anisotropy level of the peak near 740 nm. When compared to the absorption spectrum, they were seen to occur in a lower energy region distant from the prominent GaN peak near 3.4 eV (Figure 5b, marked with their approximate one-photon excitation wavelengths, 395 and 435 nm). This high degree of two-photon absorption peak anisotropy at 740 nm can be explained by the anisotropic transitions in the wurtzite GaN buffer layer, where the ground exciton states are split by crystal field spin orbit coupling.<sup>16</sup> These excitons can diffuse into IGN nanowires due to the type-I band alignment at the GaN/InGaN interface and decay through radiative recombination afterward. In contrast, the two peaks in the IGN absorption spectral region had a much lower degree of anisotropy, although these IGN nanowires also had the wurtzite structure. Comparing with pristine GaN crystals, the number of defect states is much higher in IGN nanowires. These defect states could affect the electronic absorptions parallel and perpendicular to the c-axis in this wurtzite structure. Dielectric constant mismatch in the perpendicular

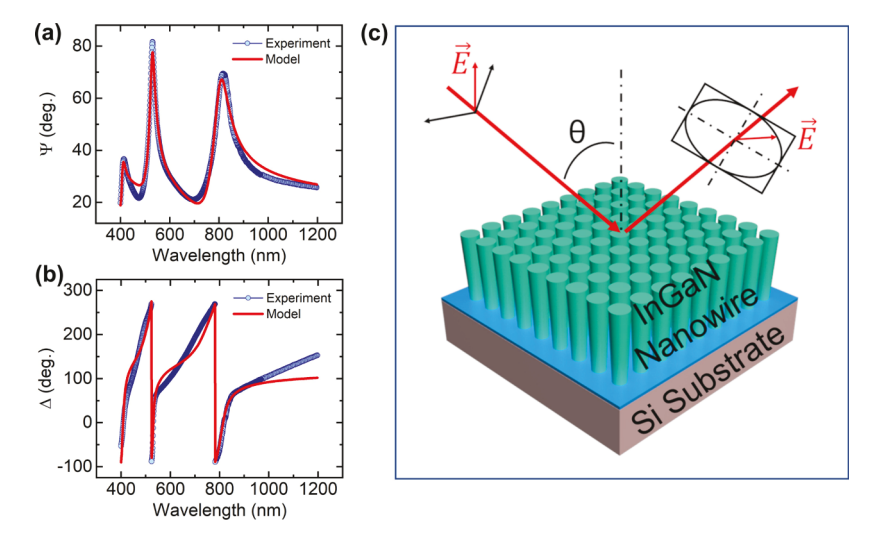


Figure 6. Ellipsometry data and modeling of IGN nanowires. (a,b) Measured (blue circles) spectral dependence of  $\Psi$  and  $\Delta$  along with model (solid red line) for IGN nanowire samples. (c) IGN sample physical model constructed (based on characterization) for ellipsometry data analyses and modeling of the optical properties.

direction also leads to reduced light absorption, <sup>17</sup> which is similar to the case of light emission mentioned above. Hence, the origin of this two-photon absorption anisotropy is similar to that of radiative recombination. A similar polarized light one-photon absorption phenomenon has been observed from InP nanowires with comparable size. <sup>35</sup>

One more noticeable difference between these two peaks and the GaN peak is that their peak FWHM was much broader, about 50 vs 20 nm. This wide inhomogeneous broadening of IGN nanowire peaks can be attributed to the large variations of the nanowires' geometry and compositions. These three peaks also have different peak heights. The peak at 790 nm was consistently higher than the peak at 870 nm. From these relative peak heights, we can qualitatively estimate the oscillator strength of each transition among IGN peaks. For the peak at 740 nm, the peak height fitting result shows large variations. Possibly, the excitation efficiency in this thin buffer layer varies among different regions.

We have observed both polarized absorption and emission from IGN nanowires grown on a Si substrate. Our results showed that in the perpendicular direction two-photon absorption and PL emission are stronger. The mechanism is due to the anisotropic crystal structure in the wurtzite phase, which results in anisotropic selection rules. Several previous studies have shown that light absorption and emission are more prominent in the parallel direction of the IGN nanowire axis. 18,36 The existence of such discrepancy indicates that many other factors can contribute to light absorption and radiative recombination. Defects are common among nanostructures. For instance, wide-bandgap wurtzite ZnO nanowires show a significant green emission peak other than the main exciton emission peak in the UV wavelength range.<sup>37</sup> The intensity of this UV peak has its maximum parallel to the c-axis, while the intensity of the green emission peak has its maximum perpendicular to the c-axis. This green emission is from trap states, where surface-trapped holes can recombine with electrons in oxygen vacancies.<sup>37</sup>

Disorder or localized states are also responsible for radiative and non-radiative recombination. <sup>38,39</sup> Atomically, IGN is inhomogeneous with many In–N condensates. These In–N condensates trap holes to form localized excitons and

radiatively recombine.<sup>38</sup> Excitons could couple to a larger density of disorder states, which can absorb light and decay non-radiatively to excitons.<sup>39</sup> It is highly possible that these disorders and localized states have different symmetry and selection rules. Donor-bound excitons and phonon-assisted optical transitions can also modify the selection rules of radiative recombination due to the impurity site symmetries and phonon symmetries.<sup>33,40</sup>

Along with the anisotropic two-photon absorption characteristics of IGN nanowires, we have investigated their wavelength-dependent tailoring of optical constants and dielectric functions. IGN nanowires' optical constants were primarily derived from SE, which quantifies the differences in amplitude and phase between linearly polarized monochromatic incident light and its oblique reflection from the IGN sample surface. The angles  $\Psi$  (azimuth) and  $\Delta$  (phase change) measured (Figure 6) from SE are connected to the microstructure and optical characteristics, as defined by  $^{41-45}$ 

$$\rho = R_{\rm p}/R_{\rm s} = \tan \Psi \exp(i\Delta) \tag{3}$$

where  $R_{\rm p}$  and  $R_{\rm s}$  are the complex reflection coefficients of the light polarized parallel and perpendicular to the plane of incidence, respectively. Based on the best fit between experimental and simulated spectra, the spectral dependencies of the ellipsometric parameters  $\Psi$  and  $\Delta$  (see Figure 6a,b, respectively) and can be fitted with the appropriate models to extract the optical constants, i.e., the refractive index (n) and extinction coefficient (k). The Levenberg–Marquardt regression procedure was applied in this instance to minimize the mean-squared error (MSE) $^{41,42}$ 

$$MSE = \frac{1}{2N - M} \sum_{i=1}^{n} \left[ \left\{ \frac{(\Psi_{exp} - \Psi_{calc})}{\sigma_{\Psi_{i}}^{exp}} \right\}^{2} + \left\{ \frac{(\Delta_{exp} - \Delta_{calc})}{\sigma_{\Delta_{i}}^{exp}} \right\}^{2} \right]$$

$$(4)$$

where  $\Psi_{\rm exp}$ ,  $\Psi_{\rm calc}$  and  $\Delta_{\rm exp}$ ,  $\Delta_{\rm calc}$  are the measured (experimental) and calculated ellipsometry functions, N is the number of measured  $\Psi$ ,  $\Delta$  pairs, M is the number of fitted

parameters in the optical model, and  $\sigma$  are standard deviations of the experimental data points.

The creation of an optical model of the sample, which often accounts for a number of discrete layers with individual optical dispersions, is necessary to extract useful physical/optical information from ellipsometry. Interfaces between the discrete layers constitute optical boundaries at which light is refracted and reflected according to the Fresnel relations. In Figure 6c, a schematic representation of the stack model that was utilized to generate spectra in order to ascertain the optical constants of IGN nanowires is presented. The IGN nanowires, the interface, and the Si substrate were located in the model as indicated. Empirical parameterization was done using the Tauc–Lorentz (TL) model, which is based on the Tauc expression for the imaginary part ( $\varepsilon_2$ ) of the dielectric function.  $\varepsilon_2$  is defined as  $\varepsilon_1^{41,42}$ 

$$\varepsilon_2(E) = \left[ \frac{A_{\rm L} E_0 C (E - E_{\rm g})^2}{(E^2 - E_0^2)^2 + C^2 E^2} \cdot \frac{1}{E} \right]$$
 (5)

where  $E_0$  is the resonance energy,  $E_{\rm g}$  represents band gap energy, E photon energy, and  $A_{\rm L}$ , C are the amplitude and broadening coefficient of  $\varepsilon_2$  peak, respectively. The aforementioned model made it possible to determine the optical constants, n and k, of the IGN nanowires. Figure 7 shows the

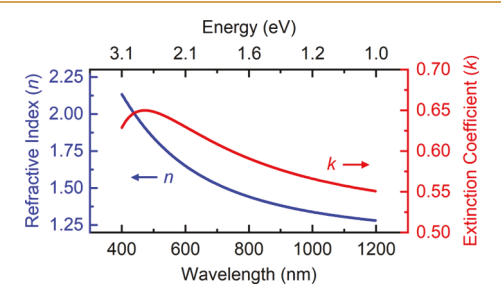


Figure 7.  $k(\lambda)$  and  $n(\lambda)$  dispersion profiles of IGN nanowires.

variation of optical constants, namely the refractive index, extinction coefficient, and dielectric function, of IGN nanowires. The TL oscillator model was used to fit the amplitude  $(\Psi)$  and phase  $(\Delta)$  components. There are not many reports on the SE analysis of typical IGN nanowires, but a few recent efforts can be found on similar nitride semiconductor thin films and nanostructures. The extracted wavelength-dependent optical constants were found to be in good agreement with the existing reports and can be analyzed further in accordance with the anisotropic luminescence data.

The spectral dependence of the n and k values, determined from SE data (Figure 7) of IGN nanowires, is typically related to the microstructure, crystallinity, and composition of the In-N, Ga-N, and In-Ga-N alloys and can be tailored accordingly to demonstrate novel optoelectronic, photonic, and photocatalytic devices.

## 4. CONCLUSIONS

Summarizing the results, we investigated the molecular beam epitaxy-produced IGN nanowires' two-photon absorption spectra. Using a home-built two-photon PL microscope and a tunable femtosecond laser to excite in the near-IR range, the IGN nanowires were studied in the 690–950 nm excitation range. The nature of polarized light absorption and emission in

IGN was studied by means of this two-photon PL microscopy. The results presented demonstrate strongly signaled polarized PL in the direction perpendicular to the c-axis of the IGN nanowires. Strong two-photon absorption was also seen above the bandgap, with excitation spectra peaks located at about 740, 790, and 870 nm. The anisotropy of the wurtzite phase of IGN nanowires may be the cause of these peaks' anisotropic response to the excitation polarization angle. While conducting this anisotropic absorption spectroscopy, we have only considered interband transitions. There are many other mechanisms that can contribute to such phenomena. One mechanism is the free carrier absorption. Once excited into conduction/valence bands, electrons/holes in different momentum valleys can further absorb light to make transitions. This process will also be anisotropic depending on the energy and momentum conservation. Theoretical and experimental studies have shown such anisotropic phenomena. 48,49 Another important mechanism is the spontaneous polarization and strain-induced polarization when growing crystals along different axes. For instance, a strong electric field is formed when growing c-plane GaN heterostructures. 50-53 Such internal electric fields will reduce oscillator strength and lower radiative recombination probability. These possible mechanisms need further investigation. In the PL process, the anisotropy could come from anisotropic excited states, such as different excitonic states in 0-dimension quantum dots.<sup>54</sup> The fundamental aspects of polarized light absorption and emission explored by this work in IGN nanowires may be useful for the future development of materials for optoelectronic device applications.

#### AUTHOR INFORMATION

## **Corresponding Authors**

Debabrata Das — Center for Advanced Materials Research (CMR) and Department of Aerospace & Mechanical Engineering, University of Texas at El Paso, El Paso, Texas 79968, United States; ◎ orcid.org/0000-0003-4326-6805; Email: ddas@utep.edu

Chunqiang Li — Department of Physics, University of Texas at El Paso, El Paso, Texas 79968, United States; orcid.org/0000-0003-1220-1611; Email: cli@utep.edu

#### **Authors**

Emma M. Sundin — Department of Metallurgical, Materials and Biomedical Engineering and Center for Advanced Materials Research (CMR), University of Texas at El Paso, El Paso, Texas 79968, United States; orcid.org/0000-0002-9251-3641

Kausik Kolluri – Department of Physics, University of California Santa Barbara, Santa Barbara, California 93106, United States

Pallab Bhattacharya — Department of Electrical Engineering and Computer Science, University of Michigan, Ann Arbor, Michigan 48109, United States

Chintalapalle V. Ramana — Center for Advanced Materials Research (CMR) and Department of Aerospace & Mechanical Engineering, University of Texas at El Paso, El Paso, Texas 79968, United States; orcid.org/0000-0002-5286-3065

Complete contact information is available at: https://pubs.acs.org/10.1021/acsaom.3c00038

#### **Author Contributions**

<sup>¶</sup>E.M.S. and D.D. contributed equally.

#### **Notes**

The authors declare no competing financial interest.

## ACKNOWLEDGMENTS

The authors acknowledge, with pleasure, support from the National Science Foundation (NSF) with NSF-PREM grant no. DMR-1827745. This material is also based upon work supported by the Air Force Office of Scientific Research under award number FA9550-18-1-0387. The work at the University of Michigan was supported by the College of Engineering under the Blue Sky Research Program.

#### REFERENCES

- (1) Li, S.; Waag, A. GaN Based Nanorods for Solid State Lighting. J. Appl. Phys. 2012, 111, 071101.
- (2) Baliga, B. J. Gallium Nitride Devices for Power Electronic Applications. Semicond. Sci. Technol. 2013, 28, 074011.
- (3) Wasisto, H. S.; Prades, J. D.; Gülink, J.; Waag, A. Beyond Solid-State Lighting: Miniaturization, Hybrid Integration, and Applications of GaN Nano- and Micro-LEDs. *Appl. Phys. Rev.* **2019**, *6*, 041315.
- (4) Vurgaftman, I.; Meyer, J. R. Band Parameters for Nitrogen-Containing Semiconductors. *J. Appl. Phys.* **2003**, *94*, 3675–3696.
- (5) Guo, W.; Zhang, M.; Banerjee, A.; Bhattacharya, P. Catalyst-Free InGaN/GaN Nanowire Light Emitting Diodes Grown on (001) Silicon by Molecular Beam Epitaxy. *Nano Lett.* **2010**, *10*, 3355–3359.
- (6) Hazari, A.; Hsiao, F. C.; Yan, L.; Heo, J.; Millunchick, J. M.; Dallesasse, J. M.; Bhattacharya, P. 1.3 μm Optical Interconnect on Silicon: A Monolithic III-Nitride Nanowire Photonic Integrated Circuit. *IEEE J. Quantum Electron.* **2017**, *53*, 1–9.
- (7) Deshpande, S.; Heo, J.; Das, A.; Bhattacharya, P. Electrically Driven Polarized Single-Photon Emission from an InGaN Quantum Dot in a GaN Nanowire. *Nat. Commun.* **2013**, *4*, 1675.
- (8) Frost, T.; Jahangir, S.; Stark, E.; Deshpande, S.; Hazari, A.; Zhao, C.; Ooi, B. S.; Bhattacharya, P. Monolithic Electrically Injected Nanowire Array Edge-Emitting Laser on (001) Silicon. *Nano Lett.* **2014**, *14*, 4535–4541.
- (9) Das, D.; Aiello, A.; Guo, W.; Bhattacharya, P. InGaN/GaN Quantum Dots on Silicon with Coalesced Nanowire Buffer Layers: A Potential Technology for Visible Silicon Photonics. *IEEE Trans. Nanotechnol.* **2020**, *19*, 571–574.
- (10) Pandey, A.; Mi, Z. III-Nitride Nanostructures for High Efficiency Micro-LEDs and Ultraviolet Optoelectronics. *IEEE J. Quantum Electron.* **2022**, 58, 1–13.
- (11) Zhang, H.; Min, J. W.; Gnanasekar, P.; Ng, T. K.; Ooi, B. S. InGaN-Based Nanowires Development for Energy Harvesting and Conversion Applications. *J. Appl. Phys.* **2021**, *129*, 121103.
- (12) Hu, J.; Li, L. S.; Yang, W.; Manna, L.; Wang, L. w.; Alivisatos, A. P. Linearly Polarized Emission from Colloidal Semiconductor Quantum Rods. *Science* **2001**, 292, 2060–2063.
- (13) Wang, J.; Gudiksen, M. S.; Duan, X.; Cui, Y.; Lieber, C. M. Highly Polarized Photoluminescence and Photodetection from Single Indium Phosphide Nanowires. *Science* **2001**, 293, 1455–1457.
- (14) Dresselhaus, G. Optical Absorption Band Edge in Anisotropic Crystals. *Phys. Rev.* **1957**, *105*, 135–138.
- (15) Birman, J. L. Some Selection Rules for Band-Band Transitions in Wurtzite Structure. *Phys. Rev.* **1959**, *114*, 1490–1492.
- (16) Casella, R. C. Symmetry of Wurtzite. Phys. Rev. 1959, 114, 1514-1518.
- (17) Ruda, H. E.; Shik, A. Polarization-Sensitive Optical Phenomena in Thick Semiconducting Nanowires. *J. Appl. Phys.* **2006**, *100*, 024314
- (18) Corfdir, P.; Feix, F.; Zettler, J. K.; Fernández-Garrido, S.; Brandt, O. Importance of the Dielectric Contrast for the Polarization of Excitonic Transitions in Single GaN Nanowires. *New J. Phys.* **2015**, *17*, 033040.

- (19) Garmire, E. Nonlinear Optics in Daily Life. Opt. Express 2013, 21, 30532–30544.
- (20) Chin, A. H.; Ahn, T. S.; Li, H.; Vaddiraju, S.; Bardeen, C. J.; Ning, C. Z.; Sunkara, M. K. Photoluminescence of GaN Nanowires of Different Crystallographic Orientations. *Nano Lett.* **2007**, *7*, 626–631.
- (21) Giblin, J.; Vietmeyer, F.; McDonald, M. P.; Kuno, M. Single Nanowire Extinction Spectroscopy. *Nano Lett.* **2011**, *11*, 3307–3311.
- (22) McDonald, M. P.; Chatterjee, R.; Si, J.; Jankó, B.; Kuno, M. Dimensional Crossover in Semiconductor Nanostructures. *Nat. Commun.* **2016**, *7*, 12726.
- (23) Aiello, A.; Das, D.; Bhattacharya, P. InGaN/GaN Quantum Dot Light-Emitting Diodes on Silicon with Coalesced Gan Nanowire Buffer Layer. *ACS Appl. Nano Mater.* **2021**, *4*, 1825–1830.
- (24) Godiksen, R. H.; Aunsborg, T. S.; Kristensen, P. K.; Pedersen, K. Two-Photon Photoluminescence and Second-Harmonic Generation from Unintentionally Doped and Semi-Insulating GaN Crystals. *Appl. Phys. B* **2017**, *123*, 270.
- (25) Fang, Y.; Yang, J.; Xiao, Z.; Wu, X.; Jia, J.; Chen, Y.; Wu, Q.; Song, Y. Ultrafast Bulk Carrier Dynamics in Various GaN Crystals at near-Infrared Wavelengths under One- and Two-Photon Absorption. *Appl. Phys. Lett.* **2019**, *114*, 112108.
- (26) Cheriton, R.; Sadaf, S. M.; Robichaud, L.; Krich, J. J.; Mi, Z.; Hinzer, K. Two-Photon Photocurrent in InGaN/GaN Nanowire Intermediate Band Solar Cells. *Commun. Mater.* **2020**, *1*, 63.
- (27) You, G.; Guo, W.; Zhang, C.; Bhattacharya, P.; Henderson, R.; Xu, J. Excitation Dependent Two-Component Spontaneous Emission and Ultrafast Amplified Spontaneous Emission in Dislocation-Free InGaN Nanowires. *Appl. Phys. Lett.* **2013**, *102*, 091105.
- (28) Kubelka, P. New Contributions to the Optics of Intensely Light-Scattering Materials. Part I. J. Opt. Soc. Am. 1948, 38, 448-457.
- (29) Makeswaran, N.; Das, D.; Zade, V.; Gaurav, P.; Shutthanandan, V.; Tan, S.; Ramana, C. V. Size-and Phase-Controlled Nanometer-Thick  $\beta$ -Ga<sub>2</sub>O<sub>3</sub> Films with Green Photoluminescence for Optoelectronic Applications. *ACS Appl. Nano Mater.* **2021**, *4*, 3331–3338.
- (30) Hahn, C.; Zhang, Z.; Fu, A.; Wu, C. H.; Hwang, Y. J.; Gargas, D. J.; Yang, P. Epitaxial Growth of InGaN Nanowire Arrays for Light Emitting Diodes. *ACS Nano* **2011**, *5*, 3970–3976.
- (31) Kuykendall, T.; Ulrich, P.; Aloni, S.; Yang, P. Complete Composition Tunability of InGaN Nanowires Using a Combinatorial Approach. *Nat. Mater.* **2007**, *6*, 951–956.
- (32) Almeida, D. B.; de Thomaz, A. A.; Carvalho, H. F.; Cesar, C. L. One- and Two-Photon Photoluminescence Excitation Spectra of CdTe Quantum Dots in a Cryogenic Confocal Microscopy Platform. *Opt. Express* **2015**, 23, 19715–19727.
- (33) Paskov, P. P.; Paskova, T.; Holtz, P. O.; Monemar, B. Polarized Photoluminescence Study of Free and Bound Excitons in Free-Standing GaN. *Phys. Rev. B: Condens. Matter Mater. Phys.* **2004**, *70*, 035210.
- (34) Mishra, A.; Titova, L. V.; Hoang, T. B.; Jackson, H. E.; Smith, L. M.; Yarrison-Rice, J. M.; Kim, Y.; Joyce, H. J.; Gao, Q.; Tan, H. H.; Jagadish, C. Polarization and Temperature Dependence of Photoluminescence from Zincblende and Wurtzite InP Nanowires. *Appl. Phys. Lett.* **2007**, *91*, 263104.
- (35) De Luca, M.; Zilli, A.; Fonseka, H. A.; Mokkapati, S.; Miriametro, A.; Tan, H. H.; Smith, L. M.; Jagadish, C.; Capizzi, M.; Polimeni, A. Polarized Light Absorption in Wurtzite InP Nanowire Ensembles. *Nano Lett.* **2015**, *15*, 998–1005.
- (36) Chen, H. Y.; Yang, Y. C.; Lin, H. W.; Chang, S. C.; Gwo, S. Polarized Photoluminescence from Single GaN Nanorods: Effects of Optical Confinement. *Opt. Express* **2008**, *16*, 13465–13475.
- (37) Hsu, N. E.; Hung, W. K.; Chen, Y. F. Origin of Defect Emission Identified by Polarized Luminescence from Aligned ZnO Nanorods. *J. Appl. Phys.* **2004**, *96*, 4671–4673.
- (38) Chichibu, S. F.; Uedono, A.; Onuma, T.; Haskell, B. A.; Chakraborty, A.; Koyama, T.; Fini, P. T.; Keller, S.; DenBaars, S. P.; Speck, J. S.; Mishra, U. K.; Nakamura, S.; Yamaguchi, S.; Kamiyama, S.; Amano, H.; Akasaki, I.; Han, J.; Sota, T. Origin of Defect-Insensitive Emission Probability in In-Containing (Al,In,Ga)N Alloy Semiconductors. *Nat. Mater.* 2006, *5*, 810–816.

- (39) Nelson, C.; Ra, Y. H.; Mi, Z.; Steel, D. G. Efficient Coupling of Disorder States to Excitons in an InGaN Nanostructure. *Phys. Rev. B* **2018**, *98*, 081201.
- (40) Toropov, A. A.; Kitaev, Y. E.; Shubina, T. V.; Paskov, P. P.; Bergman, J. P.; Monemar, B.; Usui, A. Polarization-Resolved Phonon-Assisted Optical Transitions of Bound Excitons in Wurtzite GaN. *Phys. Rev. B: Condens. Matter Mater. Phys.* **2008**, 77, 195201.
- (41) Jellison, G. E. The Calculation of Thin Film Parameters from Spectroscopic Ellipsometry Data. *Thin Solid Films* **1996**, 290–291, 40–45.
- (42) Fujiwara, H. Spectroscopic Ellipsometry: Principles and Applications; John Wiley & Sons, 2007.
- (43) Ramana, C. V.; Baghmar, G.; Rubio, E. J.; Hernandez, M. J. Optical Constants of Amorphous, Transparent Titanium-Doped Tungsten Oxide Thin Films. ACS Appl. Mater. Interfaces 2013, 5, 4659–4666.
- (44) Ramana, C. V.; Mudavakkat, V. H.; Bharathi, K. K.; Atuchin, V. V.; Pokrovsky, L. D.; Kruchinin, V. N. Enhanced Optical Constants of Nanocrystalline Yttrium Oxide Thin Films. *Appl. Phys. Lett.* **2011**, 98, 031905.
- (45) Ramana, C. V.; Utsunomiya, S.; Ewing, R. C.; Becker, U.; Atuchin, V. V.; Aliev, V. S.; Kruchinin, V. N. Spectroscopic Ellipsometry Characterization of the Optical Properties and Thermal Stability of ZrO<sub>2</sub> Films Made by Ion-Beam Assisted Deposition. *Appl. Phys. Lett.* **2008**, *92*, 011917.
- (46) Kazazis, S. A.; Papadomanolaki, E.; Androulidaki, M.; Kayambaki, M.; Iliopoulos, E. Optical Properties of InGaN Thin Films in the Entire Composition Range. *J. Appl. Phys.* **2018**, *123*, 125101.
- (47) Santos, A. J.; Lacroix, B.; Blanco, E.; Hurand, S.; Gómez, V. J.; Paumier, F.; Girardeau, T.; Huffaker, D. L.; García, R.; Morales, F. M. Simultaneous Optical and Electrical Characterization of GaN Nanowire Arrays by Means of Vis-IR Spectroscopic Ellipsometry. *J. Phys. Chem. C* **2020**, *124*, 1535–1543.
- (48) Ščajev, P.; Jarašiūnas, K.; Özgür, Ü.; Morkoç, H.; Leach, J.; Paskova, T. Anisotropy of Free-Carrier Absorption and Diffusivity in M-Plane GaN. *Appl. Phys. Lett.* **2012**, *100*, 022112.
- (49) Soltani, M.; Soref, R. Free-Carrier Electrorefraction and Electroabsorption in Wurtzite GaN. *Opt. Express* **2015**, 23, 24984–24990.
- (50) Kuokstis, E.; Chen, C. Q.; Gaevski, M. E.; Sun, W. H.; Yang, J. W.; Simin, G.; Asif Khan, M.; Maruska, H. P.; Hill, D. W.; Chou, M. C.; Gallagher, J. J.; Chai, B. Polarization Effects in Photoluminescence of C- and M-Plane GaN/AlGaN Multiple Quantum Wells. *Appl. Phys. Lett.* **2002**, *81*, 4130–4132.
- (51) Gardner, N. F.; Kim, J. C.; Wierer, J. J.; Shen, Y. C.; Krames, M. R. Polarization Anisotropy in the Electroluminescence of M-Plane InGaN—GaN Multiple-Quantum-Well Light-Emitting Diodes. *Appl. Phys. Lett.* **2005**, *86*, 111101.
- (52) Paskov, P. P.; Schifano, R.; Monemar, B.; Paskova, T.; Figge, S.; Hommel, D. Emission Properties of a-Plane GaN Grown by Metal-Organic Chemical-Vapor Deposition. *J. Appl. Phys.* **2005**, *98*, 093519.
- (53) Lai, K. Y.; Paskova, T.; Wheeler, V. D.; Grenko, J. A.; Johnson, M. A. L.; Barlage, D. W.; Udwary, K.; Preble, E. A.; Evans, K. R. Excitation Current Dependent Cathodoluminescence Study of InGaN/GaN Quantum Wells Grown on M-Plane and C-Plane GaN Substrates. *J. Appl. Phys.* **2009**, *106*, 113104.
- (54) Versteegh, M. A. M.; Reimer, M. E.; Jöns, K. D.; Dalacu, D.; Poole, P. J.; Gulinatti, A.; Giudice, A.; Zwiller, V. Observation of Strongly Entangled Photon Pairs from a Nanowire Quantum Dot. *Nat. Commun.* **2014**, *5*, 5298.